Kovove Mater. 61 2023 307–320
DOI: 10.31577/km.2023.5.307

Effect of lithium on mechanical and corrosion properties of friction stir back extruded Al-Cu-Mg alloy

Marjan Rezaee, Hamed Jamshidi Aval*

Department of Materials Engineering, Babol Noshirvani University of Technology, Shariati Avenue, Babol 47148-71167, Iran

Received 22 December 2022, received in revised form 5 May 2023, accepted 16 May 2023

Abstract

In this study, the effect of severe plastic deformation during friction stir back extrusion of Al-Cu-Mg alloy with different amounts of Li microalloying on microstructure, mechanical properties, and corrosion resistance was investigated. The Cu:Mg ratio in the Al-Cu-Mg alloy was 3.8. The results show that regardless of the amount of lithium microalloying added in the Al-Cu-Mg alloy, a significant change in the size of the dendrites, as well as the amount of secondary phase particles, and the eutectic structure formed in the inter-dendritic space, is not visible. Although with the increase of lithium percentage up to 0.5 wt.%, a slight decrease in grain size is observed in the central area and surface areas of the extruded wires, the difference in the average grain size in the three samples is not large. As the amount of lithium increases, the amount of lithium in the structure of S-Al_2CuMg precipitates increases, and finer precipices are formed. By adding 0.5 wt.% of lithium, the evidence shows that the corrosion resistance has increased by 35 %. It is also observed that the corrosion potential decreases by 7 % with the increase of lithium percentage up to 0.5 wt.%.

K e y w o r d s: friction stir back extrusion, severe plastic deformation, Al-Cu-Mg alloy, Li microalloying

1. Introduction

Precipitation-hardening aluminum alloys are widely used in various industries, such as transportation and aerospace, because of their special properties, such as special strength and high flexibility [1]. Numerous properties, especially the mechanical properties of these alloys, largely depend on the precipitates formed during the aging process, which act as a main strengthening mechanism in Al alloys [2]. It should be noted that the properties of aluminum alloys are strongly affected by the chemical composition of these alloys and the heat and mechanical treatment performed on them [3]. Various researchers have reported that the control of fraction, size, morphology, and distribution is crucial for developing advanced Al alloys with optimal mechanical properties.

Despite the existence of various methods for improving the mechanical and corrosion properties of aluminum alloys, microalloying has been introduced as an effective approach to increase the mechanical and corrosion performance of Al alloys [4]. The partial addition of alloying elements affects the thermodynamics and kinetics of precipitates and improves the properties, especially the mechanical properties of aluminum alloy. The operation of microalloy elements is summarized: Microalloy elements can easily trap vacancies because of their high vacancy-binding energy, which depends on the type of nucleation mechanism, can lead to delay or accelerate the precipitation kinetics [5]. Of course, it should be noted that the competitive behavior of different precipitates may occur and hence can lead to a different precipitation sequence [6]. Alloying elements are mainly placed at the interface of precipitates to reduce the surface energy and improve their stability [7].

The effect of adding alloy elements in small amounts has been investigated, mainly in aluminum alloys with medium strength, where the average strength of the base alloy is around 200 MPa [8]. How-

*Corresponding author: tel.: +98 11 35501808; e-mail address: h.jamshidi@nit.ac.ir

ever, it should be noted that adding microalloy elements to high-strength aluminum alloys and its effect on precipitation behavior has been a controversial process. Mainly in high-strength aluminum alloys, studies have focused on methods such as severe plastic deformation (SPD) to increase strength, and less attention has been paid to the effect of microalloy elements [9]. However, it should be noted that the application of SPD methods makes the final shape of the product not always controllable, and therefore, the use of alloying methods may be considered a better option to increase strength. Among the various alloying elements that are added to aluminum alloys, lithium is considered an important alloying element in Al alloys because of its high potential to reduce the alloy density and increasing Young's modulus [10].

Aluminum-lithium alloys (Al-Li alloys) are a set of alloys of aluminum and lithium, often also including copper and zirconium. Since lithium is the least dense elemental metal, these alloys are significantly less dense than aluminum. Commercial Al-Li alloys contain up to 2.45 % lithium by mass. However, it should be noted that fracture toughness in the Al--Li alloy is lower compared with conventional Al alloys because of a greater propensity for low-energy intergranular fracture. Lithium segregation to grain boundaries is the prime cause of low-energy intergranular fracture in Al-Li alloys. Some unsolved problems hinder the wide use of Al-Li alloys in aircraft engineering. The problems are the low thermal stability, the high anisotropy of mechanical properties, the capacity for stain localization, the high scattering of the values of fracture toughness, the low ductility in the altitudinal direction, and the deviation of fatigue crack trajectory from a straightforward direction [11]. In addition to the studies conducted on Al-Li alloys which are mainly strengthened by the T1 phase and δ' phase [12, 13], various studies [14–18] have also been conducted to investigate the effect of lithium on Al-Zn-Mg and Al-Cu-Mg based alloys and show that the addition of partial lithium can significantly affect the precipitation behavior of Al alloys. Duan et al. [19] investigated the effect of adding a small amount of lithium to an Al-Cu-Mg alloy. They reported that the addition of 0.5 wt.% of lithium resulted in a significant improvement in tensile strength without significant loss in ductility. The reason for this phenomenon was the effect of lithium addition on changing the precipitation process and the formation of very fine S-Al_2CuMg precipitates in the microstructure.

As mentioned before, one of the conventional methods for increasing the strength of high-strength aluminum alloys is the application of SPD. The application of SPD and its effect on the strengthening of aluminum alloys, including the Al-Cu-Mg alloy, have been studied by various researchers [20, 21]. One method of applying SPD that can improve the microstructure and form a uniform microstructure is the frictional stir-back extrusion (FSBE) process. In this process, the heat caused by friction is used to facilitate the creation of flow in the material. The main idea of this method was first taken by the Welding Institute in Cambridge, UK, in 1993, from the friction stir welding process [22]. The main parameters in this process are rotational speed, extrusion speed, applied force, and punch diameter. The rotational speed plays the most important role in reducing the grain size, and the punch diameter has the least contribution [23]. The results show that increasing or decreasing the rotational speed causes the appearance of defects. Cold cracks and twisting defects are observed at low rotational speeds, and hot cracks on the surface at higher rotational speeds [24]. The extrusion speed is the second parameter affecting the microstructure and mechanical properties. In applying this process to aluminum alloys, it was found that the effect of this parameter on the refinement of the microstructure is slightly more than its effect on the increase of hardness [25]. To produce a flawless extruded product, the design of the punch and die geometry plays a very important role. The details of the dimensions of the punch and die play an important role in achieving maximum efficiency, and reducing friction and power consumption [26]. Although the geometrical parameters, as mentioned before, do not have a dominant effect on the microstructure and properties, the change of these parameters can be effective in achieving the desired rotational and extrusion speeds.

Although the effect of lithium content in different ratios of Cu:Mg in Al-Cu-Mg alloys has been studied by researchers [27, 28], the effect of lithium as a microalloying element and the effect of SPD on the microstructure, mechanical properties, and corrosion of Al-Cu-Mg alloy containing lithium has not been studied. In this research, the ratio of copper to magnesium is considered to be equal to 3.8, and the effect of SPD caused by the FSBE process on the microstructure, mechanical properties, and corrosion of Al-Cu-Mg alloy containing 0.25 and 0.5 wt.% has been studied.

2. Experimental procedures

In this research, Al-Cu-Mg alloy with the copper to magnesium ratio of 3.8 has been selected as the base alloy, and the lithium element has been added to the base alloy as a micro-alloy in amounts less than 0.5 wt.%. The reason for adding lithium in amounts less than 0.5 wt.% is based on [19], where it is mentioned that in amounts less than 0.5 wt.%, it is not possible to form complex compounds and precipitates in the microstructure, and the added lithium will lead to the acceleration of the formation of S-Al_2CuMg precipitates. To manufacture the cast alloys, commer-

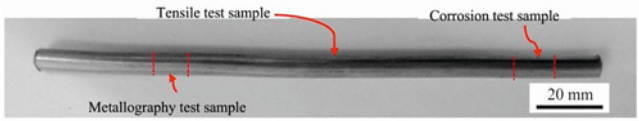

Fig. 1. The extruded wire after the FSBE process and extraction position of tensile test, metallography, and corrosion test samples.

cial AA2024 with a chemical composition of 0.18 % Si, 3.98 % Cu, 1.04 % Mg, 0.24 % Fe, 0.51 % Mn, and Al balance (wt.%) was melted in an electric resistance furnace. Next, 0.25 and 0.5 wt.% of Li were added to Al-Cu-Mg alloy using pure Al-5Li master alloy. The dissolved molten metal was subjected to gas bubbling filtration at 700 ℃ for 10 min using Ar gas. The degassed molten metal was poured into a preheated cylindrical mold at 180 ℃ (diameter 22 mm, height 200 mm). The billets for FSBE were machined to a diameter and height of 20 and 50 mm, respectively. After being heated at 495 ℃ for 24 min, the billets were friction stirred back extruded. Samples with 0, 0.25, and 0.5 wt.% of Li were labeled with C0, C25, and C50, respectively. After quenching, the samples were immediately subjected to FSBE using a punch with an outer diameter of 20 mm and length of 150 mm, in which a hole with a diameter of 7 mm was created. The extrusion process was performed at a rotational speed of 800 rpm and an extrusion speed of 20 mm min^{-1}.

After extrusion, to check the microstructure, mechanical properties, and corrosion resistance, different samples were prepared from the extruded rod, according to Fig. 1. The microstructure of the samples was etched using an etchant, including 95 ml distilled water, 1.5 ml HCl, 1 ml HF, and 2.5 ml HNO_3. The microstructure was examined using the NGF-120A optical microscope and a Philips-XL30FSEM scanning electron microscope (SEM) equipped with an EDS detector. A linear intercept technique (ASTM E112-96) was used to determine the grain sizes. In addition, a Rigaku Ultima IV X-ray diffraction machine was used for phase analysis. The hardness of the samples was measured using a KOOPA Universal (UV1) microhardness tester with a force of 100 gr and a duration time of 15 s. The tensile test was performed according to the ASTM E8 standard using a crosshead speed of 1 mm min^{-1}. To check the reproducibility of the tensile test results, three tensile samples were prepared from each wire. To check the corrosion resistance of different samples, the corrosion resistance of the cross-section of different samples was studied. To perform the corrosion test on different samples, the electrochemical test was performed by the Autolab PGSTAT204 device. Before starting the corrosion test, the samples were immersed in NaCl solution for one hour. The side surfaces of the corrosion samples were covered with resin to avoid direct contact with the corrosion solution on other surfaces. The electrochemical impedance test was performed in the frequency range of 0.1 Hz to 100 kHz. Then, all samples were kept for polarization and fixed open circuit potential to perform an electrochemical corrosion test between 250 to –250 mV. Then the electrochemical impedance test was performed at a speed of 1 mV s^{-1}.

3. Results and discussion

In Fig. 2, the microstructure of different samples before and after the extrusion process is shown. In all samples, before the extrusion process, the dendritic structure, along with the intermetallic compounds between the dendrites, are visible. As seen, regardless of the amount of lithium added to the aluminum matrix, a significant change in the size of the dendrites, as well as the amount of secondary phase particles and the eutectic structure formed in the inter-dendritic space, is not visible. After the FSBE process, the dendritic structure and the secondary phase particles in the inter-dendritic space of the dendrites are completely removed and a fine equiaxed microstructure is formed in the entire cross-section of the wire. According to previous research [29], the formation of fine and equiaxed grains after the FSBE process is related to the occurrence of dynamic recrystallization during the process.

Although with the increase of lithium percentage, a slight decrease in grain size is observed in the central area and surface areas of the three samples, the difference in the average grain size in the three samples is not large. The average grain size of extruded samples C0, C25, and C50 is 19.54 ± 2.42, 19.94 ± 3.84, and 21.03 ± 2.35 μm, respectively. The measurement of wire surface temperature in the three samples does not show a significant difference. The maximum temperature of the wire surface in samples C0, C25, and C50 is 451, 454, and 456 ℃, respectively. According to [30], two factors of temperature and plastic strain are effective in forming recrystallized grains. In such a way that with increasing temperature or decreasing plastic strain, the recrystallized grain size increases. Considering that the plastic strain during the process cannot be easily measured experimentally, the plastic strain during the process was predicted according to the method proposed in [31], and the maximum plastic strain values were obtained in the samples C0, C25, and C50 as 21.34, 22.05, 21.89, respectively. According to the values of plastic strain and temperature measured during the FSBE process, which are not significantly different, it may be possible to justify the slight difference in the average grain size of the three samples after the extrusion process. Another important point is the difference in grain size on the surface and

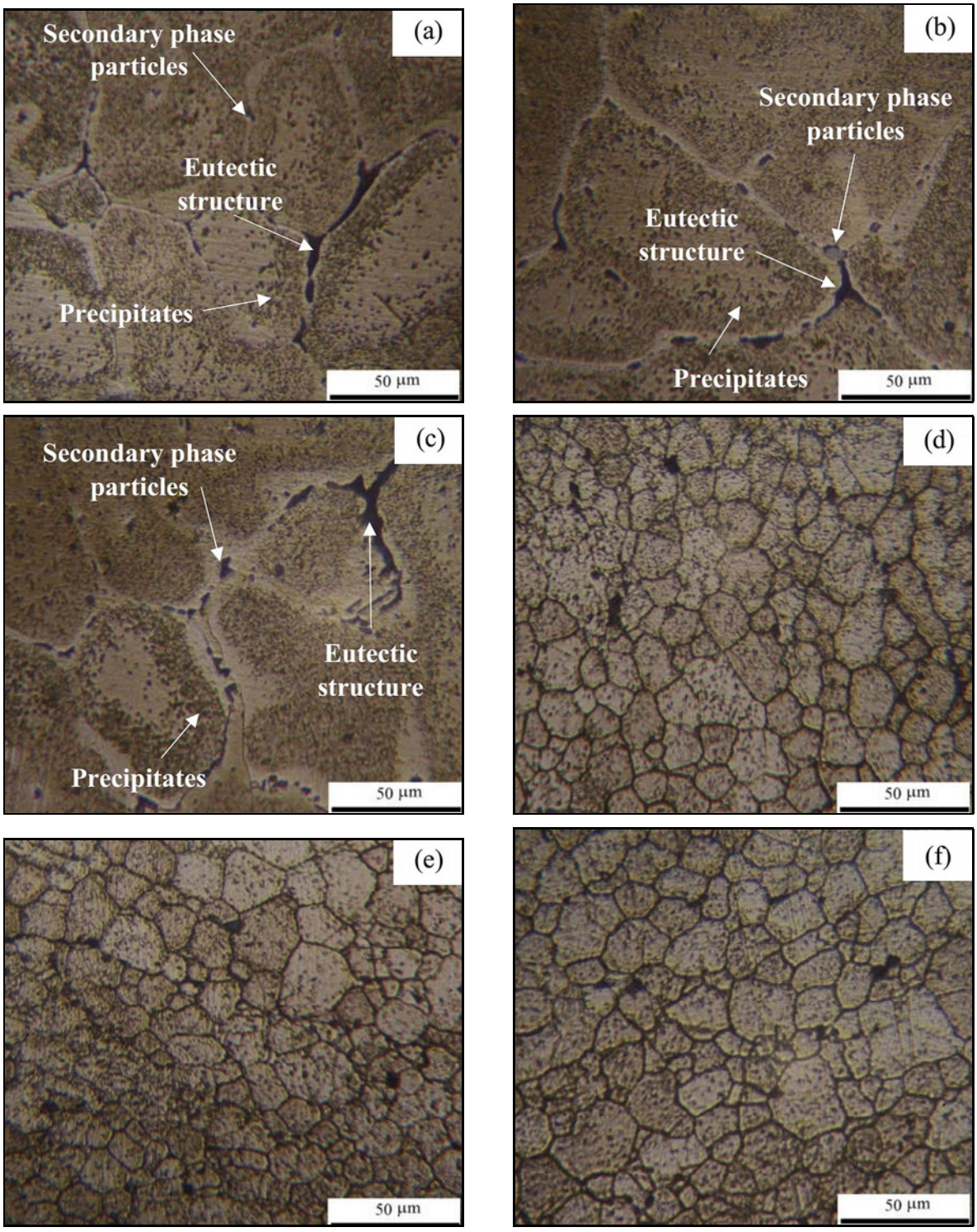

Fig. 2. The optical microscopy images of: (a) sample C0, (b) sample C25, (c) sample C50 before FSBE and (d) sample C0, (e) sample C25, (f) sample C50 after FSBE.

the center of all three samples, so the grain size on the surface of the wire is larger than the center zone. The reason for this phenomenon can be justified according to the results of temperature and plastic strain obtained from experimental measurement and simulation. According to the simulation results, the temperature on the surface of the wire is higher than in the center zone. Also, the plastic strain in the surface areas is much higher than in the center zone. Similar results concerning temperature changes and plastic strain have been reported by other researchers [32]. Considering the higher temperature in the surface ar-

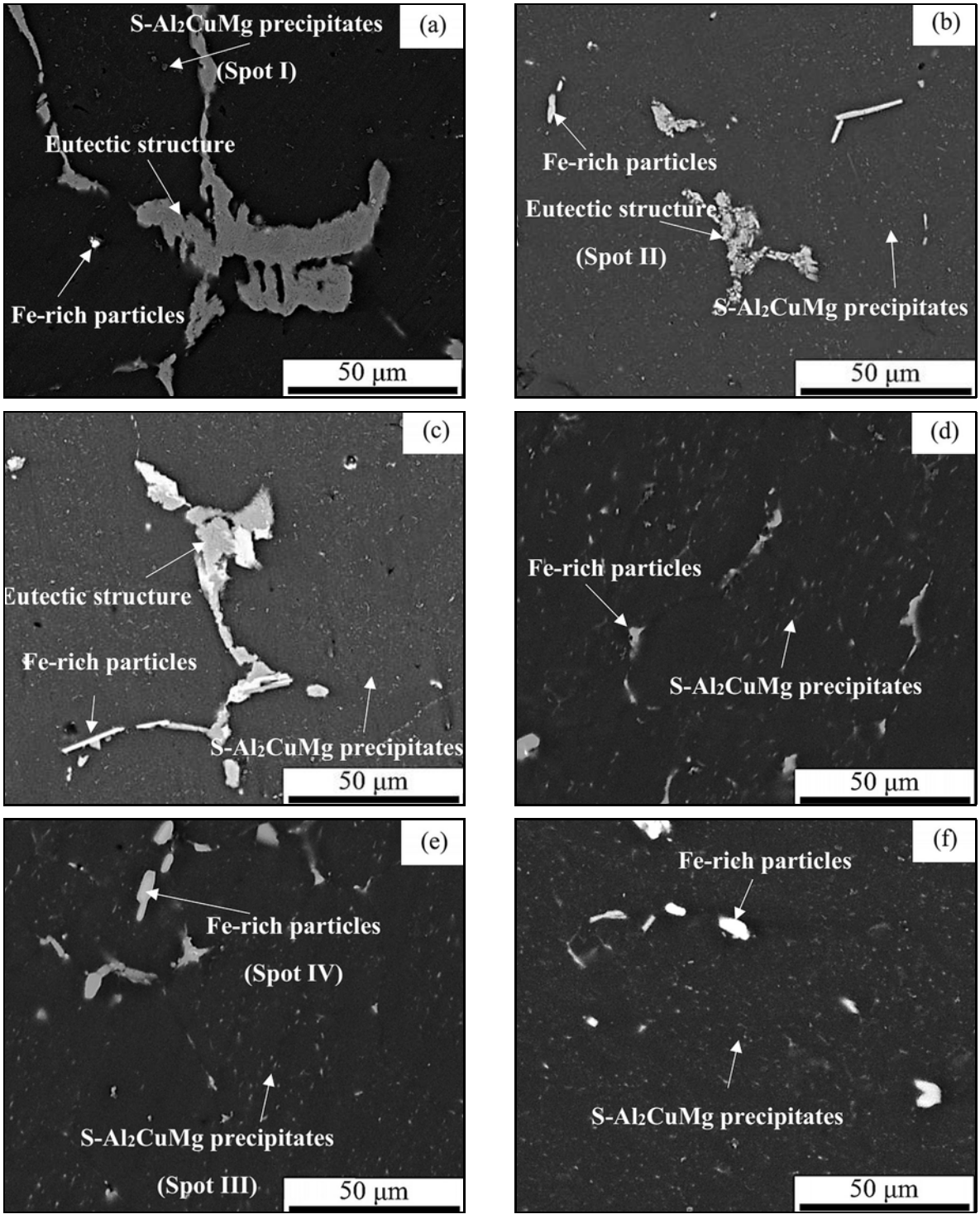

Fig. 3. The SEM images of extruded samples; (a) sample C0, (b) sample C25, c) sample C50 before FSBE and (d) sample C0, (e) sample C25, (f) sample C50 after FSBE.

eas, it can be said that the effect of temperature on grain growth in the surface areas has been dominant in plastic strain. Because of the conflict between the effect of temperature and plastic strain, a higher temperature in the surface areas causes grain growth and the formation of coarser grains in the surface areas.

To be a more precise study of the precipitates and secondary phase particles formed in the microstructure of different samples, the SEM images of the microstructure in the center of the different samples are shown in Fig. 3. Also, the results of the EDS analysis of precipitates and secondary phase particles are

Table 1. EDS analysis result of different points marked in Fig. 3

Element (Atomic %)	Al	Mg	Cu	Li	Fe	Mn
Spot I	74.03	10.04	15.67	–	0.14	0.12
Spot II	64.40	15.98	19.45	–	0.12	0.05
Spot III	73.98	11.45	14.32	0.12	0.08	0.05
Spot IV	78.97	0.07	0.40	–	14.11	6.45

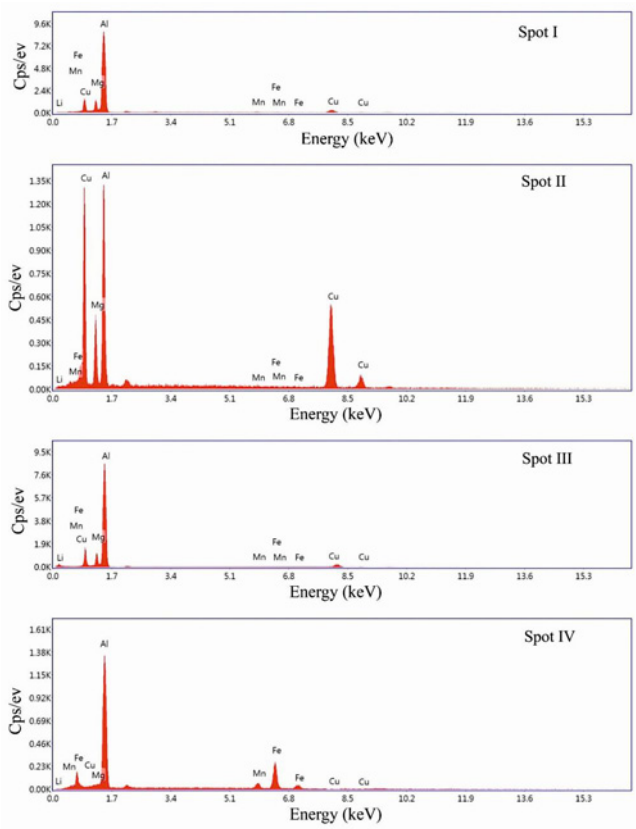

Fig. 4. The EDS results of different points marked in Fig. 3.

reported in Fig. 4 and Table 1. According to the results of EDS analysis and composition of precipitates and secondary phase particles reported by other researchers [19], the microstructure of the alloys in the as-cast state mainly includes Fe-rich particles, eutectic structure, and Cu-Mg-rich precipitates. Meanwhile, in the samples containing lithium, a little lithium can also be seen in the Cu-Mg-rich precipitates. The secondary phase particles and precipitates observed in the extruded structure are like the as-cast sample, with the difference that the eutectic structure is not visible in the extruded samples.

As the amount of lithium increases, the amount of lithium in the structure of Cu-Mg-rich precipitates increases. Comparing the atomic percentage of Cu and Mg in the Cu-Mg rich precipitates with the atomic percentage of Cu and Mg in S-Al_2CuMg precipitates shows that these precipitates are probably the S--Al_2CuMg precipitates, which has also been reported in other research. As seen, the usual precipitates in Al-Li alloys are not visible in the microstructure of samples containing lithium. According to [33], it has been reported that lithium replaces part of the magnesium element in the structure of the S-Al_2CuMg precipitates. According to the investigations, no traces of T1 and δ precipitates were observed in the microstructure. According to [34–36], the absence of these precipitates is related to the low amounts of lithium additive, in such a way that because of the high amounts of Cu and Mg present in the microstructure, the S precipitates formation overcomes the formation of lithium-rich precipitates and particles. In this situation, since the substitution of lithium instead of magnesium leads to a decrease in the enthalpy of the formation of S precipitates, the added lithium in the structure replaces part of the magnesium in the structure of S precipitates. It is noteworthy that after extrusion, a finer and higher number of precipitates are formed in sample C50 compared to samples C25 and C0. The average size of S precipitates has been obtained by SEM images, due to the limitation of imaging at high magnifications. According to [19], the addition of lithium through the mechanism of the Li-Vacancy complex leads to an increase in the nucleation of S precipitates and the formation of fine precipitates with high thermal stability. An important factor in controlling the kinetics of precipitation is the solute-vacancy binding energy. The binding energy of the Li-Vacancy couple is 0.25 ± 0.03 eV [37]; this value is high enough to allow Li atoms to trap vacancies during the quenching and to nucleate dislocation loops.

The X-ray diffraction results of different samples can be seen in Figure 5. The results show that only the peak related to the aluminum matrix appeared in the diffraction, and there is no trace of precipitates or secondary phase particles observed in the SEM images. The reason for this finding is probably because of the formation of small amounts of these precipitates and secondary phase particles, which cannot be detected by X-ray diffraction. One of the proposed strengthening mechanisms in aluminum alloys is strengthening through crystallographic texture. The formation of the preferred texture in aluminum alloys can affect the strength and ductility of these alloys. Among the important textures that can increase strength or

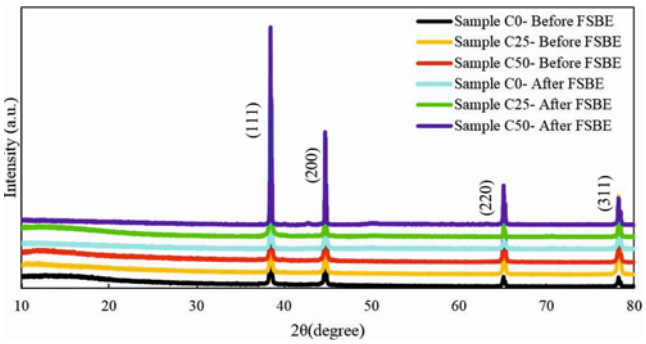

Fig. 5. XRD pattern related to as-cast and extruded samples.

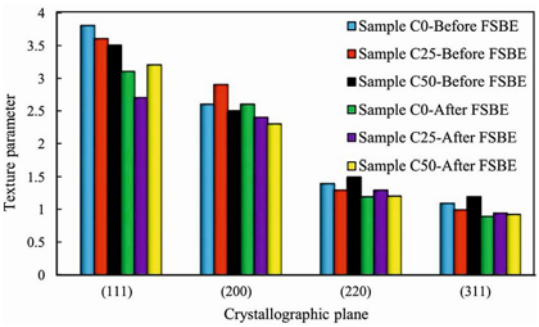

Fig. 6. The texture parameters of as-cast and extruded samples.

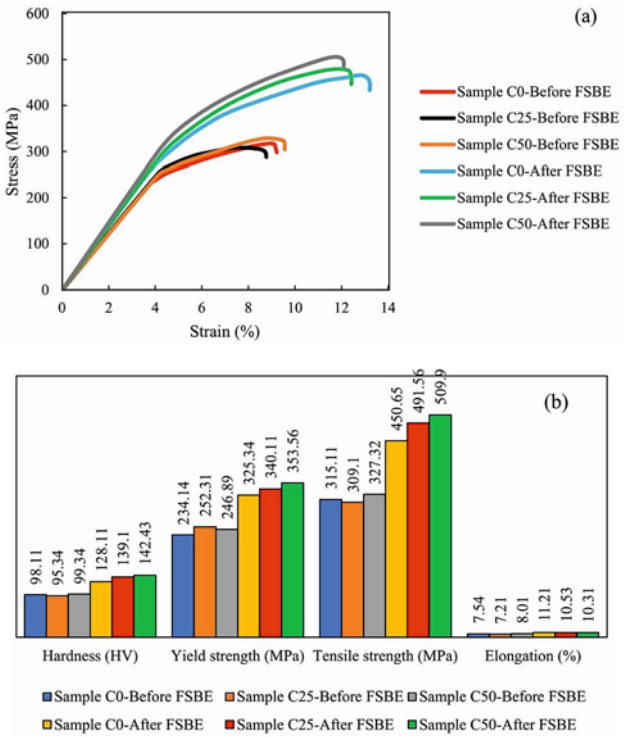

Fig. 7. a) stress-strain curve of different samples, b) hardness and tensile test results.

ductility in aluminum alloys are {100} and {111}. To investigate the formation of preferred texture in different samples, according to Eq. (1), the texture parameter of different samples was calculated. The texture parameter (TP_{hkl}) was derived from I_{0hkl} (intensity of (hkl) in an Al alloy with random orientation) and was then used to determine the orientation of the grains. The texture parameter is described as follows [38]:

$$TP_{hkl} = \frac{I_{hkl}/I_{0hkl}}{\frac{1}{n}\sum_{1}^{n} I_{hkl}/I_{0hkl}}. \quad (1)$$

The texture parameter results of different samples are presented in Fig. 6. As seen, in both series of as-cast and extruded samples, the addition of lithium changes the texture parameters. By adding lithium to the Al-Cu-Mg alloy, the {110} texture is weakened, and the {100} texture is strengthened. Although the intensity of the texture has dropped significantly in the extruded samples compared to the as-cast sample with the same composition, the difference in the crystallographic texture can be seen in the extruded samples with the addition of lithium. Meanwhile, in the extruded samples, the intensity of the {100} texture is strengthened. Based on [39, 40], the {100} and {111} texture reinforcement increases strength and ductility in aluminum, respectively. Therefore, it can be expected that balancing these two components can achieve remarkable strength and ductility in aluminum.

Figure 7 shows the hardness and strength results of different samples. Also, the fracture surface of extruded samples is shown in Fig. 8. According to the hardness and tensile test results, two general findings can be stated: first, the hardness and strength, and elongation are improved by performing the FSBE process. Second, with the addition of lithium, the amount of hardness and strength, and elongation increases. The effect of lithium on extruded samples is clear compared to as-cast samples. The improvement in hardness, strength, and elongation in the extruded sample compared to the as-cast sample can be attributed to the removal of casting defects such as porosity, as well as the formation of fine and uniform grains along with fine precipitates in the extruded sample. The increase in hardness and strength in the extruded sample with the increase of lithium can be related to the effect of lithium in increasing the nucleation kinetics of S precipitates. Of course, it should be noted that besides strengthening through precipitates, probably the formation of texture increases the ductility in the extruded sample with an increase in the percentage of lithium. The lack of significant change in hard-

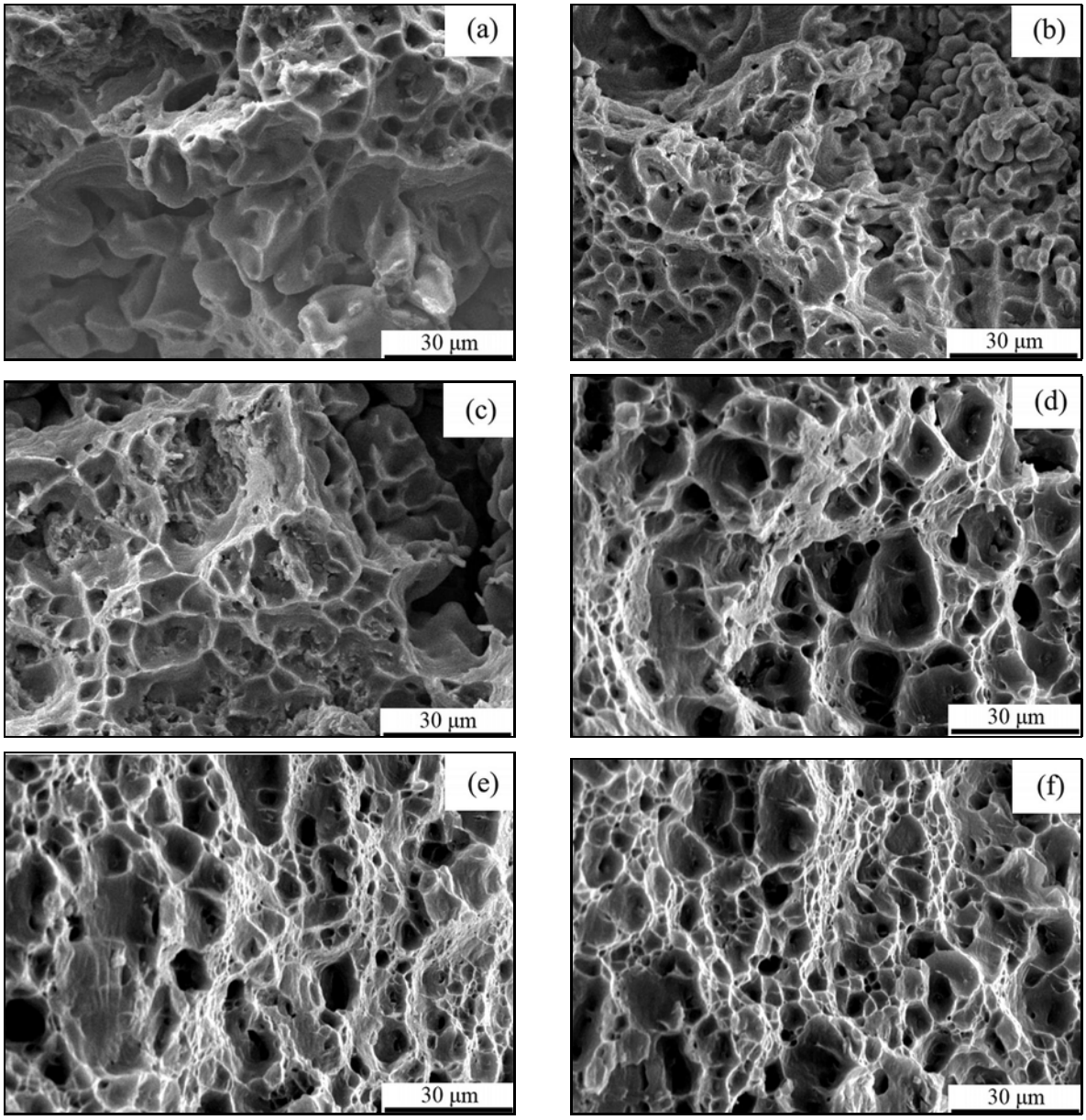

Fig. 8. The SEM images of the fracture surface of samples; (a) sample C0, (b) sample C25, (c) sample C50 before FSBE and (d) sample C0, (e) sample C25, (f) sample C50 after FSBE.

ness, strength, and elongation in the as-cast sample with the change in lithium percentage can probably be related to defects and low percentages of lithium so that the effect of porosity and defects in reducing strength is far greater than the effect of lithium micro-alloy.

The mechanical properties of a metal depend on the movement of dislocations. The easier the dislocations move, the lower the strength and the easier the deformation of the material. Creation of solid solution, grain size reduction, formation of secondary phases, strain hardening, and texture strengthening are among the strengthening mechanisms of materials [41]. In addition to grain size strengthening (GS), other mechanisms such as solid solution strengthening (SS), dispersion strengthening (DS), and precipitation strengthening (PS) will probably contribute to the overall strength. According to [42, 43], the strength of a precipitation-strengthened aluminum alloy can be defined:

$$\sigma_{\mathrm{z}} = \sigma_0 + \sigma_{\mathrm{ss}} + \sigma_{\mathrm{gs}} + \sigma_{0\mathrm{r}} + \sigma_{\mathrm{d}}, \tag{2}$$

where σ_0 is the yield stress of pure Al (taken as 35 MPa [44]), σ_{ss} is the solid solution strengthening, σ_{gs} is the grain size strengthening, and $\sigma_{0\mathrm{r}}$ is the Orowan strengthening, which comprises both DS and PS. The associated Orowan strengthening contribution can be

estimated by [45]:

$$\Delta\sigma_{\text{orowan}} = M\frac{0.4Gb}{\pi\sqrt{1-\vartheta}}\frac{\ln\left(\frac{2\bar{r}}{b}\right)}{\lambda_{\text{p}}}, \qquad (3)$$

where G is the shear modulus, which is 27 GPa for Al, b is the Burgers vector, M is the Taylor factor (∼3 for randomly oriented fcc polycrystals), υ is 0.33, $\bar{r} = r\sqrt{2/3}$ is the mean radius of a circular cross-section in a random plane for spherical particles/precipitates, r is the mean radius of the particles/precipitates, and λ_{p} is the average particles/precipitates spacing. As seen, by increasing the density of precipitates and decreasing the distance between them, and decreasing their size, the contribution of the Orowan mechanism increases. Therefore, it can be expected that by increasing the percentage of lithium, the contribution of the Orowan mechanism will increase with the decrease in the size of the precipitates and the distance between the precipitates. It should be noted that the contribution of strengthening through dislocations in extruded samples is small. Because of dynamic recrystallization during the process, most of the dislocations in the structure have disappeared, and practically the effect of strengthening through dislocations is small. The grain-boundary strengthening mechanism is usually described by the Hall-Petch equation. According to this equation, with decreasing grain size the strengthening through grain boundaries increases. Considering that the significant grain size difference is not observed in the samples with different lithium percentages, it can be said that the contribution of this mechanism in strengthening the extruded samples and creating different strength values is small.

However, the strengthening mechanism through a solid solution is also effective in a precipitation-strengthened aluminum alloy. According to [46–48], the solid solution strengthening arises from Cu, Mg, and Mn as the principal alloying elements in the base alloy used in this study, which is estimated as:

$$\sigma_{\text{ss}} = \sum_{i=\text{element}} k_i \times C_i^m, \qquad (4)$$

where C_i is the concentration of species i in the solid solution, k_i is the corresponding strengthening related to the solute-dislocation interaction that depends on the differences in the radii of the alloying and matrix elements [49], and m is a constant. Gazizov et al. [50] show that the ratio of the strengthening mechanism through Orowan strengthening is 4–5 times higher than the strengthening mechanism through the solid solution. Therefore, it can be mentioned that strengthening through a solid solution is less effective than Orowan strengthening. According to the above descriptions, it can be said that the role of strengthening through the Orowan mechanism in the strength difference between extruded samples is far more than other mechanisms.

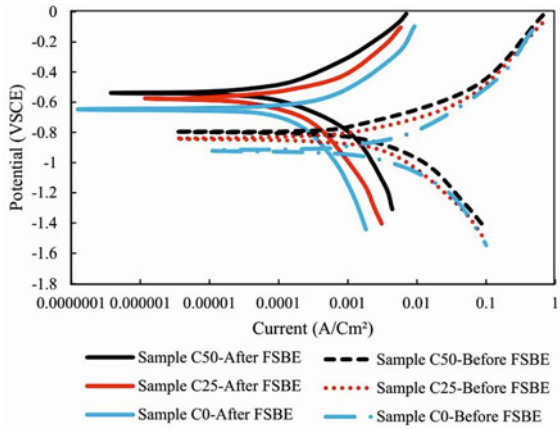

Fig. 9. Polarization curves of different samples.

Figure 9 shows the polarization curves of the as-cast and extruded samples. As seen, there is no significant difference in the rate and current of corrosion among the as-cast samples. Meanwhile, with the increase in the amount of lithium, the corrosion resistance and corrosion current in the extruded samples have increased and decreased, respectively. Adding 0.5 wt.% of lithium shows that the corrosion resistance has increased by 35 %. It is also observed that the corrosion potential decreases with the increase in lithium percentage. By reducing the corrosion potential, the resistance to pitting corrosion can be expected to increase. The high i_{corr} value in the samples with lower Li content is attributed to the coalescence of fine precipitates into coarser precipitates fewer and concentrating only in some portions of the alloy, creating nonuniform distribution and precipitate-free zones (PFZs). The improved corrosion resistance of sample C50 is related to the formation of fine-strengthening precipitates uniformly distributed throughout the alloy, avoiding the formation of PFZs [51, 52]. EIS has been popularly used in corrosion as a powerful method to study the surface condition of metals in aggressive environments. It can characterize, in terms of electrical measurements, a chemical process occurring at the electrode/electrolyte interface. EIS gives information about the response of a circuit to an alternating current (I) or voltage (V) as a function of frequency (f). Nyquist plots are frequency-independent, providing information about the charge transfer resistance (R_{ct}) and the solution resistance (R_{s}) in a corrosive medium. The inhibition of charge transfer is represented by R_{ct}. The compact native oxide layer on the surface retards the transport of corrosive ions to interact with the substrate. The charge transfer process occurs only at the electrode-electrolyte interface [51].

Table 2. The measurements made after fitting the experimental EIS data

Sample no.	Rs ($\Omega\,cm^2$)	$R1$ ($\Omega\,cm^2$)	CPE1 ($F\,cm^{-2}$)	$n1$	$R2$ ($\Omega\,cm^2$)	CPE2 ($F\,cm^{-2}$)	$n2$	R_T ($\Omega\,cm^2$)	χ-squared
C0-before FSBE	12.09	5.00E–03	4.02E–11	0.956	53.11	5.03E–05	0.785	45.32	0.074
C25-before FSBE	12.32	4.30E–03	4.98E–11	0.945	52.89	4.97E–05	0.689	47.11	0.072
C50-before FSBE	12.78	5.60E–03	5.89E–11	0.903	54.93	5.67E–05	0.653	48.09	0.067
C0-after FSBE	28.09	3.21	3.21E–03	0.785	110.34	0.00045	0.502	100.09	0.00124
C25-after FSBE	32.11	4.67	4.32E–03	0.711	121.45	0.00034	0.432	121.45	0.00112
C50-after FSBE	35.89	5.02	3.09E–03	0.672	129.93	0.00021	0.401	134.89	0.00098

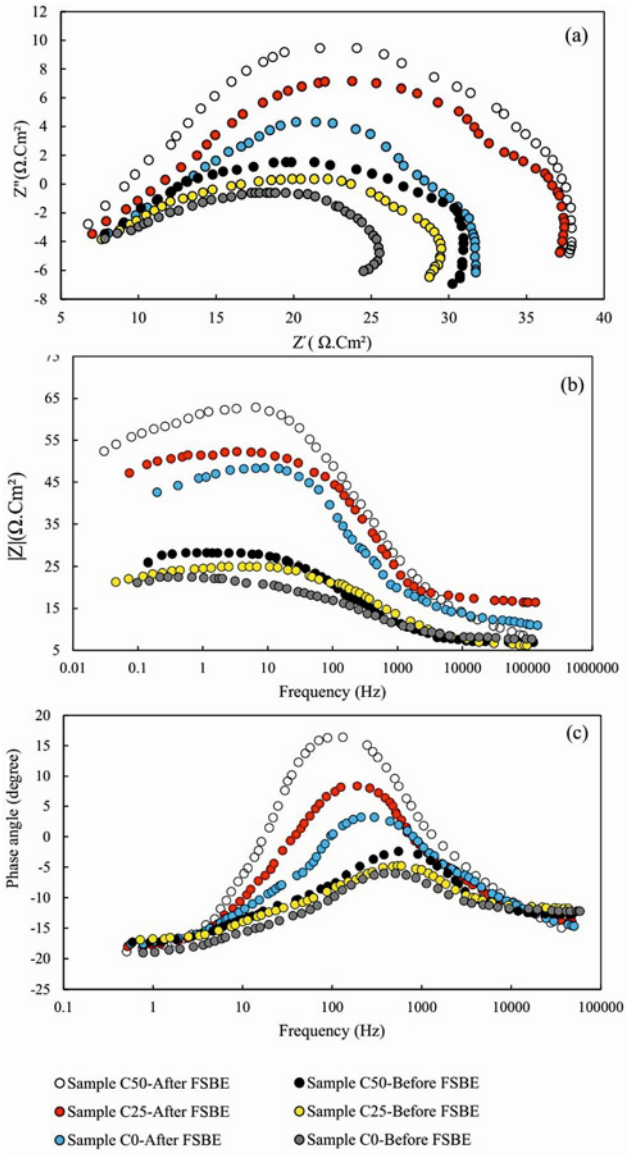

Fig. 10. (a) Nyquist diagram, (b) Bode plots, and (c) phase plots of different extruded samples.

The Nyquist plots (Fig. 10) of the extruded samples exhibit two capacitive loops, which are also reflected in the Bode impedance plots in Fig. 10, revealing the formation of two complex oxide layers on the surface in the chloride solution environment. The corrosion process of the extruded samples can be explained based on the equivalent circuits shown in Fig. 10. In the equivalent circuits, the capacitance is replaced by a constant phase element (CPE, impure capacitance) because of dispersion effects induced by the microscopic roughness of the sample surface. The double-layer and corrosive layer capacitance are coupled to the constant-phase components CPE1 and CPE2, respectively, at the substrate/electrolyte interface [53, 54]. The impedance of CPE is determined by the values of Y and n (0–1) [55]:

$$\mathrm{ZCPE} = \frac{1}{Y\,(j\omega)^n}, \tag{5}$$

where the letters Y and n stand for the dispersion index and non-ideal capacitance, respectively. For $n = 1$, CPE corresponds to an ideal capacity. The total resistance RT (RT = R1 + R2) values of the samples C0, C25, and C50 are 100.09, 121.45, and 134.89 $\Omega\,cm^2$, respectively.

Based on the fitting parameters in Table 2, the greatest RT value indicates the slowest corrosion rate, and sample C50 has the best corrosion resistance. Figure 10 displays the samples' phase curves. Each sample exhibits a consistent decline in phase angle, indicating the passivation layer and a decline in the protective properties with time and frequency. The highest and greatest phase angle indicates a considerable electrochemical resistance and further supports the creation of a high-density oxide film [56].

The corrosion tendency increases with the precipitation of S anodic precipitates in the grain boundaries or with the depletion of Cu from the surrounding matrix [57]. The coarse S precipitates, especially along the grain boundaries, leading to a large amount of material loss and finally resulting in the fallout of the grains. The corrosion surface of different samples is shown in Fig. 11, and related EDS results are reported in Table 3. The EDS results of the particles reveal the enrichment of Cu by selective dissolution of the S-phase concerning the PFZs and the matrix. By increasing Li content, the extent of corrosion damage

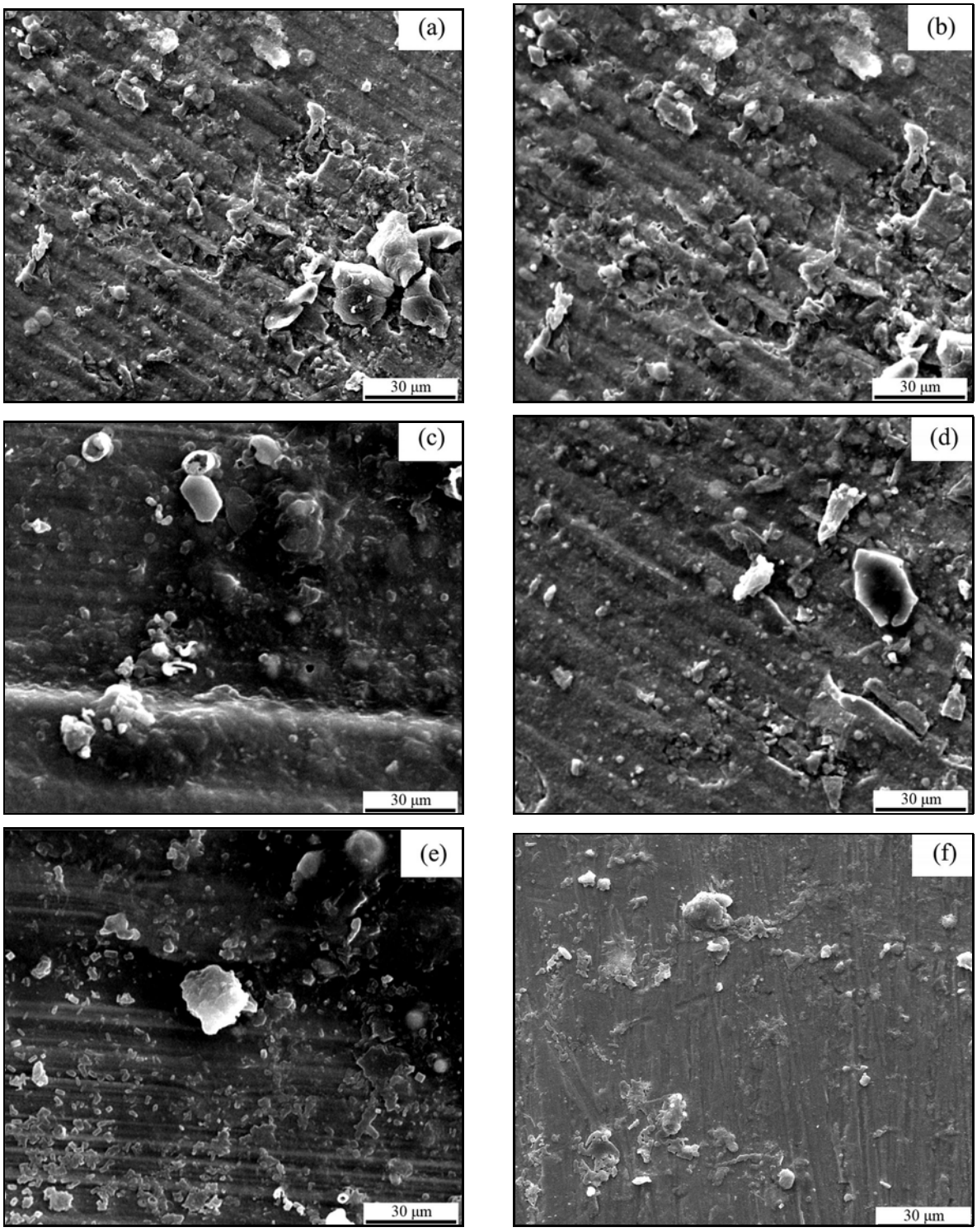

Fig. 11. The SEM images of the corrosion surface of samples: (a) sample C0, (b) sample C25, (c) sample C50 before FSBE and (d) sample C0, (e) sample C25, (f) sample C50 after FSBE.

is homogeneous, because of the uniform distribution of precipitates, as evident from the SEM image. Another important point regarding the corrosion results is that the corrosion voltage is higher in the extruded samples compared to the as-cast sample. Because of the shearing process and large strains associated with the FSBE process, the initial grain boundaries and their unique arrangement of precipitates were destroyed. The SPD during the FSBE process in effect "desensitizes" the grain boundaries and the dominant failure mode appears to be pitting, which is associated with the constituent particles [58].

Table 3. Chemical composition of corrosion surface of different samples (wt.%)

Sample label	Al	Cu	Mg	Na	Cl	O
C0-before FSBE	16.75	3.12	0.92	21.05	24.05	34.11
C25-before FSBE	22.83	3.05	0.56	19.02	22.45	32.09
C50-before FSBE	26.5	2.98	0.89	16.87	18.09	34.67
C0-after FSBE	43.43	3.03	0.78	13.09	14.56	25.11
C25-after FSBE	46.62	3.21	0.94	12.89	13.56	22.78
C50-after FSBE	44.82	3.67	0.86	12.45	12.11	26.09

4. Conclusions

The effect of lithium microalloying on mechanical and corrosion properties of friction stir back extruded Al-Cu-Mg alloy with Cu:Mg ratio 3.8 was investigated. The main findings are:

– After the FSBE process, the dendritic structure and the secondary phase particles in the interdendritic space of the dendrites are completely removed, and a fine equiaxed microstructure is formed.

– The grain size on the surface of the wire is larger than the center zone. It can be said that the effect of temperature on grain growth in the surface areas has been dominant in plastic strain.

– The microstructure of the alloys in the as-cast state mainly includes Mn-Fe-rich particles, eutectic structure, and Cu-Mg-rich precipitates. Meanwhile, in the samples containing lithium, a little lithium can also be seen in the Cu-Mg-rich precipitates.

– The hardness, strength, and elongation are improved by performing the FSBE process. Also, with the addition of lithium up to 0.5 wt.%, the hardness, yield strength, and ultimate tensile strength of FSBE processed samples increases by 11, 9, and 13 %, respectively.

– By adding 0.5 wt.% of lithium, the results show that the corrosion resistance has increased by 35 %. It is also observed that the corrosion potential decreases by 7 % with the increase of lithium percentage up to 0.5 wt.%. The corrosion voltage is higher in the extruded samples compared to the as-cast sample.

References

[1] P. Rambabu, N. Eswara Prasad, V. Kutumbarao, R. Wanhill, Aluminium alloys for aerospace applications, Aerospace Materials and Material Technologies: Volume 1: Aerospace Materials, Indian Institute of Metals Series, Springer, Singapore (2017) 29–52. https://doi.org/10.1007/978-981-10-2134-3_2

[2] J. Chen, E. Costan, M. Van Huis, Q. Xu, H. Zandbergen, Atomic pillar-based nanoprecipitates strengthen AlMgSi alloys, Science 312 (2006) 416–419. https://doi.org/ 10.1126/science.1124199

[3] K. Buchanan, K. Colas, J. Ribis, A. Lopez, J. Garnier, Analysis of the metastable precipitates in peak-hardness aged Al-Mg-Si (-Cu) alloys with differing Si contents, Acta Materialia 132 (2017) 209–221. https://doi.org/10.1016/j.actamat.2017.04.037

[4] E. Gariboldi, P. Bassani, M. Albu, F. Hofer, Presence of silver in the strengthening particles of an Al-Cu-Mg-Si-Zr-Ti-Ag alloy during severe overaging and creep, Acta Materialia 125 (2017) 50–57. https://doi.org/10.1016/j.actamat.2016.11.056

[5] M. Werinos, H. Antrekowitsch, T. Ebner, R. Prillhofer, P. J. Uggowitzer, S. Pogatscher, Hardening of Al-Mg-Si alloys: Effect of trace elements and prolonged natural aging, Materials & Design 107 (2016) 257–268. https://doi.org/10.1016/j.matdes.2016.06.014

[6] C. R. Hutchinson, S. P. Ringer, Precipitation processes in Al-Cu-Mg alloys microalloyed with Si, Metallurgical and Materials Transactions A 31 (2000) 2721–2733. https://doi.org/10.1007/BF02830331

[7] S.J. Kang, T.-H. Kim, C.-W. Yang, J. I. Lee, E. S. Park, T. W. Noh, M. Kim, Atomic structure and growth mechanism of T1 precipitate in Al-Cu-Li-Mg-Ag alloy, Scripta Materialia 109 (2015) 68–71. https://doi.org/10.1016/j.scriptamat.2015.07.020

[8] C. Li, G. Sha, B. Gun, J. Xia, X.F. Liu, Y. Wu, N. Birbilis, S. Ringer, Enhanced age-hardening response of Al–4Mg–1Cu (wt.%) microalloyed with Ag and Si, Scripta Materialia 68 (2013) 857–860. https://doi.org/10.1016/j.scriptamat.2013.02.009

[9] I. F. Mohamed, T. Masuda, S. Lee, K. Edalati, Z. Horita, S. Hirosawa, K. Matsuda, D. Terada, M. Z. Omar, Strengthening of A2024 alloy by high-pressure torsion and subsequent aging, Materials Science and Engineering A 704 (2017) 112–118. https://doi.org/10.1016/j.msea.2017.07.083

[10] R. J. Rioja, J. Liu, The evolution of Al-Li base products for aerospace and space applications, Metallurgical and Materials Transactions A 43 (2012) 3325–3337. https://doi.org/10.1007/s11661-012-1155-z

[11] V. Zakharov, Some problems of the use of aluminum-lithium alloys, Metal Science and Heat Treatment 45 (2003) 49–54. https://doi.org/10.1023/A:1023904314848

[12] F. W. Gayle, W. T. Tack, G. Swanson, F. H. Heubaum, J. R. Pickens, Composition and anisotropy in Al-Cu-Li-Ag-Mg-Zr alloys, Scripta Metallurgica et Materialia 30 (1994) 761–766. https://doi.org/10.1016/0956-716X(94)90195-3

[13] K. Kumar, F. Heubaum, The effect of Li content on the natural aging response of Al Cu Li Mg Ag Zr alloys, Acta Materialia 45 (1997) 2317–2327. https://doi.org/10.1016/S1359-6454(96)00360-6

[14] P. Bai, T. Zhou, P. Liu, Y. Zhang, C. Chen, Effects of lithium addition on precipitation in Li-containing

Al-Zn-Mg-Cu alloy, Materials Letters 58 (2004) 3084–3087. https://doi.org/10.1016/j.matlet.2004.05.048
[15] M. Starink, N. Gao, N. Kamp, S. Wang, P. Pitcher, I. Sinclair, Relations between microstructure, precipitation, age-formability and damage tolerance of Al--Cu-Mg-Li (Mn, Zr, Sc) alloys for age forming, Materials Science and Engineering A 418 (2006) 241–249. https://doi.org/10.1016/j.msea.2005.11.023
[16] Y. Wang, R. Wu, N. Turakhodjaev, M. Liu, Microstructural evolution, precipitation behavior and mechanical properties of a novel Al-Zn-Mg-Cu-Li-Sc--Zr alloy, Journal of Materials Research 36 (2021) 740–750. https://doi.org/10.1557/s43578-020-00005-4
[17] M. J. Starink, I. Sinclair, N. Gao, N. Kamp, P. J. Gregson, P. Pitcher, A. Levers, S. Gardiner, Development of new damage tolerant alloys for age-forming, In: Materials Science Forum, Trans. Tech. Publ. 2002, pp. 601–606. https://doi.org/10.4028/www.scientific.net/MSF.396-402.601
[18] Y. Koshino, M. Kozuka, S. Hirosawa, Y. Aruga, Comparative and complementary characterization of precipitate microstructures in Al-Mg-Si (-Li) alloys by transmission electron microscopy, energy dispersive X-ray spectroscopy and atom probe tomography, Journal of Alloys and Compounds 622 (2015) 765–770. https://doi.org/10.1016/j.jallcom.2014.10.199
[19] S. Y. Duan, L. K. Huang, S. H. Yang, Z. Zhou, S. J. Song, X. B. Yang, Y. Z. Chen, Y. J. Li, G. Liu, F. Liu, Uncovering the origin of enhanced strengthening in Li-added Al-Cu-Mg alloys, Materials Science and Engineering A 827 (2021) 142079. https://doi.org/10.1016/j.msea.2021.142079
[20] I. Nikulin, S. Malopheyev, A. Kipelova, R. Kaibyshev, Effect of SPD and friction stir welding on microstructure and mechanical properties of Al-Cu--Mg-Ag sheets, Materials Letters 66 (2012) 311–313. https://doi.org/10.1016/j.matlet.2011.08.104
[21] T. Kvačkaj, J. Bidulská, R. Kočiško, R. Bidulský, Effect of severe plastic deformation on the properties and structural developments of high purity Al and Al-Cu-Mg-Zr aluminium alloy, Aluminium Alloys, Theory and Applications (2011) 3–26. https://doi.org/10.5772/14425
[22] W. Tang, A. P. Reynolds, Production of wire via friction extrusion of aluminum alloy machining chips, Journal of Materials Processing Technology 210 (2010) 2231–2237. https://doi.org/10.1016/j.jmatprotec.2010.08.010
[23] Y. Chen, Q. Wang, J. Peng, C. Zhai, W. Ding, Effects of extrusion ratio on the microstructure and mechanical properties of AZ31 Mg alloy, Journal of Materials Processing Technology 182 (2007) 281–285. https://doi.org/10.1016/j.jmatprotec.2006.08.012
[24] E. Meza-García, J. Bohlen, S. Yi, D. Letzig, V. Kräusel, D. Landgrebe, K. Kainer, Influence of alloying elements and extrusion process parameter on the recrystallization process of Mg-Zn alloys, Materials Today: Proceedings 2 (2015) S19–S25. https://doi.org/10.1016/j.matpr.2015.05.004
[25] C. Wang, X. Wang, H. Chang, K. Wu, M. Zheng, Processing maps for hot working of ZK60 magnesium alloy, Materials Science and Engineering A 464 (2007) 52–58. https://doi.org/10.1016/j.msea.2007.03.003
[26] S. Fatemi-Varzaneh, A. Zarei-Hanzaki, H. Beladi, Dynamic recrystallization in AZ31 magnesium alloy, Materials Science and Engineering A 456 (2007) 52–57. https://doi.org/10.1016/j.msea.2006.11.095
[27] M. Rezaei, H. Jamshidi Aval, Effect of Cu/Mg ratio on microstructure and corrosion resistance of Al-Cu--Mg-Li cast alloy during non-isothermal aging, Metals and Materials International (2023). https://doi.org/10.1007/s12540-022-01363-w
[28] M. Rezaei, H. Jamshidi Aval, Effect of Li micro--alloying on microstructure and corrosion resistance of non-isothermal aged Al-Cu-Mg cast alloy with different Cu/Mg ratios, International Journal of Metalcasting (2023). https://doi.org/10.1007/s40962-022-00933-3
[29] P. Motavallian, S. M. Rabiee, H. J. Aval, Investigation of microstructure and corrosion behavior of AZ91/64SiO_2-31CaO-5P_2O_5 composite wire fabricated by friction stir back extrusion, Surface and Coatings Technology (2023) 129451. https://doi.org/10.1016/j.surfcoat.2023.129451
[30] F. J. Humphreys, M. Hatherly, Recrystallization and Related Annealing Phenomena, Elsevier, 2012. https://doi.org/10.1016/B978-0-08-044164-1.X5000-2
[31] P. Motavallian, S. M. Rabiee, H. Jamshidi Aval, Fabrication of new gradient AZ91-bioactive glass composite using friction stir back extrusion, Materials Today Communications 35 (2023) 105808. https://doi.org/10.1016/j.mtcomm.2023.105808
[32] A. Jahani, H. Jamshidi Aval, M. Rajabi, R. Jamaati, Effects of Ti_2SnC MAX phase reinforcement content on the properties of copper matrix composite produced by friction stir back extrusion process, Materials Chemistry and Physics 299 (2023) 127497. https://doi.org/10.1016/j.matchemphys.2023.127497
[33] S. Y. Duan, Z. Le, Z. K. Chen, Z. Gao, J. H. Chen, W. Q. Ming, S. Y. Li, C. L. Wu, N. Yan, Li-atoms-induced structure changes of Guinier-Preston--Bagaryatsky zones in AlCuLiMg alloys, Materials Characterization 121 (2016) 207–212. https://doi.org/10.1016/j.matchar.2016.09.037
[34] A. Sodergren, D. J. Lloyd, The influence of lithium on the ageing of A 7000 series alloy, Acta Metallurgica 36 (1988) 2107–2114. https://doi.org/10.1016/0001-6160(88)90312-4
[35] B. C. Wei, C. Q. Chen, Z. Huang, Y. G. Zhang, Aging behavior of Li containing Al–Zn–Mg-Cu alloys, Materials Science and Engineering A 280 (2000) 161–167. https://doi.org/10.1016/S0921-5093(99)00684-X
[36] Y. J. Gu, A. Wahab, Z. Huang, Y. G. Zhang, C. Q. Chen, The structure transformation in an Al-Li-Zn--Mg-Cu-Zr alloy, Materials Science and Engineering A 316 (2001) 39–45. https://doi.org/10.1016/S0921-5093(01)01258-8
[37] S. Ceresara, A. Giarda, A. Sanchéz, Annealing of vacancies and ageing in Al-Li alloys, The Philosophical Magazine: A Journal of Theoretical Experimental and Applied Physics 35 (1977) 97–110. https://doi.org/10.1080/14786437708235975
[38] W. Gong, K. Aizawa, S. Harjo, R. Zheng, T. Kawasaki, J. Abe, T. Kamiyama, N. Tsuji, Deformation behavior of as-cast and as-extruded $Mg_{97}Zn_1Y_2$ alloys during compression, as tracked by in situ neutron diffraction, International Journal of Plasticity 111 (2018) 288–306. https://doi.org/10.1016/j.ijplas.2018.08.001

[39] K. Yoshida, T. Ishizaka, M. Kuroda, S. Ikawa, The effects of texture on formability of aluminum alloy sheets, Acta Materialia 55 (2007) 4499–4506. https://doi.org/10.1016/j.actamat.2007.04.014
[40] Y. Wen, W. Yunxin, Effects of temperature and pressure on elastic properties of single crystal aluminum in different crystal orientations, Physica Status Solidi B 257 (2020) 2000434. https://doi.org/10.1002/pssb.202000434
[41] G. E. Dieter, D. J. Bacon, Mechanical Metallurgy, McGraw-Hill, New York, 1976.
[42] K. Ma, H. Wen, T. Hu, T. D. Topping, D. Isheim, D. N. Seidman, E. J. Lavernia, J. M. Schoenung, Mechanical behavior and strengthening mechanisms in ultrafine grain precipitation-strengthened aluminum alloy, Acta Materialia 62 (2014) 141–155. https://doi.org/10.1016/j.actamat.2013.09.042
[43] T. Shanmugasundaram, M. Heilmaier, B. S. Murty, V. S. Sarma, On the Hall-Petch relationship in a nanostructured Al-Cu alloy, Materials Science and Engineering A 527 (2010) 7821–7825. https://doi.org/10.1016/j.msea.2010.08.070
[44] M. Bauccio, ASM Metals Reference Book, ASM International, 1993.
[45] B. Cao, S. P. Joshi, K. Ramesh, Strengthening mechanisms in cryomilled ultrafine-grained aluminum alloy at quasi-static and dynamic rates of loading, Scripta Materialia 60 (2009) 619–622. https://doi.org/10.1016/j.scriptamat.2008.12.026
[46] R. Labusch, Statistical theories of solid solution hardening, Acta Metallurgica 20 (1972) 917–927. https://doi.org/10.1016/0001-6160(72)90085-5
[47] C. Varvenne, G. P. M. Leyson, M. Ghazisaeidi, W. A. Curtin, Solute strengthening in random alloys, Acta Materialia 124 (2017) 660–683. https://doi.org/10.1016/j.actamat.2016.09.046
[48] Ø. Ryen, B. Holmedal, O. Nijs, E. Nes, E. Sjölander, H.-E. Ekström, Strengthening mechanisms in solid solution aluminum alloys, Metallurgical and Materials Transactions A 37 (2006) 1999–2006. https://doi.org/10.1007/s11661-006-0142-7
[49] J. R. Davis, Aluminum and aluminum alloys, ASM International, 1993.
[50] M. Gazizov, R. Kaibyshev, Precipitation structure and strengthening mechanisms in an Al-Cu-Mg-Ag alloy, Materials Science and Engineering A 702 (2017) 29–40. https://doi.org/10.1016/j.msea.2017.06.110
[51] P. Laxman Mani Kanta, V. Srivastava, K. Venkateswarlu, S. Paswan, B. Mahato, G. Das, K. Sivaprasad, K. G. Krishna, Corrosion behavior of ultrafine-grained AA2024 aluminum alloy produced by cryorolling, International Journal of Minerals, Metallurgy, and Materials 24 (2017) 1293–1305. https://doi.org/10.1007/s12613-017-1522-2
[52] R. P. Wei, C.-M. Liao, M. Gao, A transmission electron microscopy study of constituent-particle-induced corrosion in 7075-T6 and 2024-T3 aluminum alloys, Metallurgical and Materials Transactions A 29 (1998) 1153–1160. https://doi.org/10.1007/s11661-998-0241-8
[53] E. Mena-Morcillo, L. Veleva, Degradation of AZ31 and AZ91 magnesium alloys in different physiological media: Effect of surface layer stability on electrochemical behaviour, Journal of Magnesium and Alloys 8 (2020) 667–675. https://doi.org/10.1016/j.jma.2020.02.014
[54] J. Wasserbauer, M. Buchtík, J. Tkacz, S. Fintová, J. Minda, L. Doskočil, Improvement of AZ91 alloy corrosion properties by duplex Ni-P coating deposition, Materials 13 (2020) 1357. https://doi.org/10.3390/ma13061357
[55] Y. Cubides, D. Zhao, L. Nash, D. Yadav, K. Xie, I. Karaman, H. Castaneda, Effects of dynamic recrystallization and strain-induced dynamic precipitation on the corrosion behavior of partially recrystallized Mg–9Al–1Zn alloys, Journal of Magnesium and Alloys 8 (2020) 1016–1037. https://doi.org/10.1016/j.jma.2020.09.005
[56] A. Abbas, S.-J. Huang, Investigating the synergic effects of WS2 and ECAP on degradation behavior of AZ91 magnesium alloy, Coatings 12 (2022) 1710. https://doi.org/10.3390/coatings12111710
[57] R. Buchheit, R. Grant, P. Hlava, B. Mckenzie, G. Zender, Local dissolution phenomena associated with S phase (Al_2CuMg) particles in aluminum alloy 2024-T3, Journal of the Electrochemical Society 144 (1997) 2621. https://doi.org/10.1149/1.1837874
[58] J. Brunner, N. Birbilis, K. Ralston, S. Virtanen, Impact of ultrafine-grained microstructure on the corrosion of aluminium alloy AA2024, Corrosion Science 57 (2012) 209–214. https://doi.org/10.1016/j.corsci.2011.12.016